### Title
Sensitivity of Mammalian Cone Photoreceptors to Infrared Light




### Authors
Vinberg, Frans
Palczewska, Grazyna
Zhang, Jianye
et al.



### Publication Date
2019-09-01

### DOI
10.1016/j.neuroscience.2019.07.047

Peer reviewed

HHS Public Access

Author manuscript

*Neuroscience*. Author manuscript; available in PMC 2020 September 15.

Published in final edited form as:

*Neuroscience*. 2019 September 15; 416: 100–108. doi:10.1016/j.neuroscience.2019.07.047.

# Sensitivity of Mammalian Cone Photoreceptors to Infrared Light

**Frans Vinberg**[a,1], **Grazyna Palczewska**[a,2], **Jianye Zhang**[3], **Katarzyna Komar**[4,5], **Maciej Wojtkowski**[5,6], **Vladimir J. Kefalov**[7], **Krzysztof Palczewski**[3,*]

[1]John A. Moran Eye Center, University of Utah, 65 Mario Capecchi Drive, Salt Lake City, UT 84132, USA [2]Polgenix, Inc., Department of Medical Devices, 5171 California Ave., Suite 150, Irvine, CA USA 92617 [3]Gavin Herbert Eye Institute, Department of Ophthalmology, University of California, Irvine, CA USA 92697 [4]Institute of Physics, Faculty of Physics, Astronomy and Informatics, Nicolaus Copernicus University in Torun, Grudziadzka 5, 87-100, Torun, Poland [5]Baltic Institute of Technology, Al. Zwyciestwa 96/98, 81-451, Gdynia, Poland [6]Department of Physical Chemistry of Biological Systems, Institute of Physical Chemistry, Polish Academy of Sciences, Kasprzaka Str. 44/52 01-224, Warsaw, Poland [7]Department of Ophthalmology and Visual Sciences, Washington University School of Medicine 660 S. Euclid Avenue, Saint Louis, MO 63110, USA

## Abstract

Two-photon vision arises from the perception of pulsed infrared (IR) laser light as color corresponding to approximately half of the laser wavelength. The physical process responsible for two-photon vision in rods has been delineated and verified experimentally only recently. Here, we sought to determine whether IR light can also be perceived by mammalian cone photoreceptors via a similar activation mechanism. To investigate selectively mammalian cone signaling in mice, we used animals with disabled rod signal transduction. We found that, contrary to the expected progressive sensitivity decrease based on the 1-photon cone visual pigment spectral template, the sensitivity of mouse cone photoreceptors decreases only up to 800 nm and then increases at 900 nm and 1000 nm. Similarly, in experiments with the parafoveal region of macaque retinas, we found that the spectral sensitivity of primate cones diverged above the predicted 1-photon spectral sensitivity template beyond 800 nm. In both cases, efficient detection of IR light was dependent on minimizing the dispersion of the ultrashort light pulses, indicating a non-linear 2-photon activation process. Together, our studies demonstrate that mammalian cones can be activated by near IR light by a nonlinear 2-photon excitation. Our results pave the way for the creation of a 2-photon IR-based ophthalmoscope for the simultaneous imaging and functional testing of human retinas as a novel tool for the diagnosis and treatment of a wide range of visual disorders.

[*]Corresponding author: Krzysztof Palczewski, Ph.D., Phone: (949) 824-6527, Fax: 949-824-4015, kpalczew@uci.edu.
[a]These authors contributed equally



Conflict of interests

K.P. is Chief Scientific Officer at Polgenix, Inc. K.P. is also an inventor of the U.S. patent no. 7,706,863 and U.S. patent no. 8,346,345, whose values may be affected by this publication. G.P. is an employee of Polgenix, Inc.

**Keywords**

Cone visual pigment; two-photon absorption; infrared vision; transretinal electrophysiology; phototransduction

## INTRODUCTION

Light-sensitive photoreceptors of the retina consist of rod and cone cells that contribute to different aspects of our vision. The distribution of rods and cones across the retina is not uniform. In the human retina, the fovea is localized in the center of the retina, within which the foveola consists exclusively of cones, whereas toward the periphery rods comprise the majority of photoreceptors. The parafovea, immediately surrounding the fovea, is contiguous with the perifovea. All three regions, fovea, parafovea and perifovea constitute the macula (about 5.5 mm in diameter) (Curcio et al., 1987; Curcio et al., 1990; Mustafi et al., 2009; Masland, 2012). It is within this region where age-related as well as juvenile forms of retinal degeneration take place, such as age-related macular degeneration (AMD) and Stargardt disease, respectively (Ambati and Fowler, 2012). The periphery of the retina is associated with such diseases as retinitis pigmentosa (RP), a genetically inherited progressive retinal degeneration (Rivolta et al., 2002). Thus, interrogating the function of both rods and cones in different regions of the retina is critical for monitoring the initiation and progression of these and other degenerative process as well as the efficacy of therapeutic interventions.

The range of wavelengths over which humans are able to perceive light (visible range) is governed by the absorption spectra of human rod and cone visual pigments (Crawford, 1949; Kraft et al., 1993). Although the practical visible light range for human vision is considered to be 400 to 720 nm, numerous reports exist of perception in the near infrared. Thus, it is now accepted that, given a sufficiently powerful source of IR light, humans can respond to radiation at wavelengths as long as 1355 nm (Griffin et al., 1947; Walraven and Leebeek, 1963; Sliney et al., 1976; Dmitriev et al., 1979). This result suggests that individual photoreceptors can be activated by near IR light and generate electric responses to drive visual perception. It was recently shown that in the case of mammalian rods, including human, the detection of near IR light can occur by a mechanism of 2-photon excitation (Palczewska et al., 2014b). However, whether mammalian cone photoreceptors can also be activated by near IR light has not been studied in detail and the possible mechanism by which IR light activates mammalian cone photoreceptors has not been determined.

In this study, we sought to determine whether mouse and primate cones respond to near IR light and to identify the possible mechanism by which mammalian cone pigments are activated by IR radiation. We present evidence that similar to rods, mouse and primate cones also are responsive to pulsing IR light by a 2-photon excitation. These results point to the possibility of developing an IR-based 2P ophthalmoscope for simultaneous imaging and functional testing of human retinas that would advance ophthalmic examination and the diagnosis and treatment of a wide range of human visual disorders affecting rod and cone photoreceptors.

# EXPERIMENTAL PROCEDURES

## Animals

All mice were housed in the Animal Resource Center at the School of Medicine, Case Western Reserve University, where they were maintained on a normal mouse chow diet under complete darkness for at least 24 h before Electroretinogram (ERG) recordings or in a 12 h light (~10 lux)/12 h dark cyclic environment. Animals studies were reviewed and approved by the Case Western Reserve University, School of Medicine Institutional Animal Care and Use Committee, located in Cleveland OH. These studies (Assurance number A-3145–01) conformed to both the recommendations of the American Veterinary Medical Association Panel on Euthanasia and the Association for Research in Vision and Ophthalmology. Wild-type (WT), C57BL/6 mice were obtained from The Jackson Laboratory (Bar Harbor, ME). *Gnat1*$^{-/-}$ mice, kindly provided by Janis Lem (Tufts University, Boston), were maintained on C57Bl/6J background and free of the *rd8* mutation.

## Ex vivo electrophysiology and 2P imaging

**Measurement system configuration—**E*x vivo* ERG light responses were recorded from isolated retina samples of mice or macaque monkeys as described previously (Palczewska et al., 2014b). Infrared (IR) stimuli at 730 – 1000 nm were provided by a tunable Ti:Sapphire laser (Chameleon Vision S, Coherent, Santa Clara, CA) delivering 75 fs pulses at an 80 MHz frequency. Reference data at 561 nm were collected with a diode pumped solid-state (DPSS) laser (Lasos, Jena, Germany). Rod transducin-α-subunit knockout (*Gnat1*$^{-/-}$) mice and monkey retinas were used to assess cone physiology. The experimental protocol was optimized for detecting small signals from cones that can be over 100-fold less sensitive to light than fully dark-adapted mouse rods. We used Ames' medium (Sigma-Aldrich, St. Louis, MO) heated to 37 °C, continuously bubbled with carbogen (95% $O_2$ and 5% $CO_2$), and delivered at a rate of 1 mL/min over a 6–10 $mm^3$ volume above the retina (solution exchange rate ~2 $s^{-1}$). This medium was shown previously to provide larger and more sensitive photoreceptor responses in mice as compared to standard media such as Locke's or Ringer's solutions (Azevedo and Rieke, 2011; Vinberg and Kefalov, 2015). The photoreceptor component of the ERG signal was isolated by adding 100 μM Barium Chloride (Sigma-Aldrich, St. Louis, MO) and 40 μM DL-AP4 (Catalog No. 0101, Tocris Bioscience) to the perfusion medium (Heikkinen et al., 2008). A new specimen holder was designed and constructed to allow simultaneous imaging and electrophysiological recording (see Figs. 1A–B). This holder provided a short transparent path for the laser beam through a thin cover slip (VWR No. 1 ½) and only ~0.2 mm layer of perfusion solution above the retina, thus maximizing the photon count delivered to the photoreceptors and minimizing light wavefront alterations. Finally, 2P imaging with low power (Palczewska et al., 2019), allowed us to accurately focus the laser beam on the photoreceptor layer of the retina. 2P imaging was performed in situ, using 730 nm light and the same objective (0.25 NA, 10x) and the specimen holder employed for collecting electrophysiological data (Fig. 1C). The stability of recordings was tested in separate experiments and we observed less than 10% reduction in the maximal response amplitude of the *Gnat1*$^{-/-}$ mouse retinas in 1 hour following the initial 15 min period of stabilization of the responses after the retinas were placed in the specimen holder.

Trigger, provided by the 2P microscope operating in the electrophysiology mode, was used to ensure synchronization between the start of collecting electrophysiological data with the use of UBA-4200 DC amplifier (LKC Technologies, Gaithersburg, MD) and the stimulus provided by the Ti:Sapphire or DPSS laser. Sensitivity (S) was determined by dividing the amplitude of a response to a dim flash ($R_{dim}$), producing <30% of the maximal saturated response $R_{max}$, by the stimulus intensity (I) in photons $\mu m^{-2}$ and further normalized by $R_{max}$ determined at 561 nm.

$$S = R_{dim}/(I \times R_{max}) \times 100\% . \quad (1)$$

Because of the high speed of the scan (128 lines at 16,000 lines/s over a 0.738 × 0.738 mm area) and a relatively short 10 ms scan duration time as compared to the photoreceptor integration time, and the fact that the beam was focused on the photoreceptor layer of the retina, we approximated the stimulus intensity as:

$$I = \frac{P\Delta t}{A} / \frac{hc}{\lambda}, \quad (2)$$

where P is the laser power at the specimen, A is the 0.738 × 0.738 mm scanning area on the sample, Δt is the scan time (typically 10 ms) and hc/λ is the energy of a photon. During the electrophysiological measurements, we were able to focus on the outer segments as verified by the 2P imaging with 730 nm, with the back aperture of the objective overfilled. Full width half maximum (FWHM) of the focused spot for two-photon excitation, in the transverse direction, FWHM(xy), and in the axial direction, FWHM(z), were estimated based on (Zipfel et al., 2003) and at 730 nm were equal to: FWHM(xy)=1.1 μm, FWHM(z)=19 μm; at 1000 nm they were equal to FWHM(xy)=1.5 μm, FWHM(z)=26 μm.

The laser output was calibrated twice a day. First, at least 45 min after turning on all equipment for electrophysiology measurements and allowing the system to equilibrate with the laser power, and then again in the middle of the day. Average laser power was adjusted with microscope software controlling an integrated EOM, and measured for each wavelength and setting of the EOM at the sample plane with PM100D power meter equipped with S121C sensor calibrated from 400–1100 nm (Thorlabs, Newton, NJ).

**Mouse and macaque retina sample preparation—**Mouse retinas were dissected under dim red light immediately after euthanasia as described previously (Vinberg et al., 2014). Before euthanasia mice were kept in complete darkness for at least 12 h. Enucleated cynomolgus macaque (*Macaca fascicularis*, male, 3.5 y/o) eyes were obtained from Ricerca

Biosciences (Painesville, OH, USA). Preparation of dark-adapted macular samples from these retinas was accomplished in two ways. The left eye was placed in a light-tight bottle filled with $O_2$-saturated Ames' media immediately after enucleation performed under bright surgical light. The macular retina sample from the right eye was prepared immediately after enucleation under normal room light. The cornea, lens and part of the vitreous were carefully removed to avoid retinal detachment. A 6 mm retina-RPE-sclera sample with the fovea, recognized by its darker pigmentation, was punched through the vitreous (Premier Uni-Punch, #P16112240). Under dim red light, the macula/fovea neural retina then was peeled off the retinal pigmented epithelium (RPE) and sclera and placed into 5 mL of Ames' media containing 100 μM 11-*cis*-retinal. The left eye and the right macular retina sample were then transported for 1 h to the location where the electrophysiology and imaging experiments were done. The right macular retina sample was placed immediately in a fresh 5 mL of Ames' media inside a light-tight box saturated with 95% $O_2$/5% $CO_2$. The macula/fovea sample from the left eye was prepared on site just as the right macula sample but under dim red light instead to keep it dark-adapted (this eye was kept intact in darkness for a total of 1.5 h to allow pigment regeneration via the RPE visual cycle). In both punched 6 mm macula-fovea samples, the fovea was not in the center. Our *ex vivo* ERG recording experiments were confined to the 0.5 mm diameter circle determined by the electrode channel diameter of the specimen holder (Figs. 1A and 1B). This area was within the parafovea as was confirmed by 2P imaging performed after the electrophysiological recording (Fig. 5).

## Retinoid analyses

Portions of the macaque retina, RPE and retina attached to RPE that were not used for ERG recordings were saved for high-performance liquid chromatography (HPLC) analyses and frozen to −80°C at the time of completion of ERG measurements. Immediately before HPLC analyses, tissue was thawed on wet ice and homogenized in 1 mL of 10 mM sodium phosphate buffer, pH 8.0, containing 50% methanol (v/v) and 100 mM hydroxylamine. Then 2 mL of 3 M sodium chloride was added. The resulting mixture was extracted twice with 3 mL of ethyl acetate. The combined organic layers were dried *in vacuo*, reconstituted in 400 μL of hexanes, and 100 μL of this extract were injected into a normal-phase HPLC unit (Agilent Sil, 5 μm, 4.6 × 250 mm; Agilent Technologies, Santa Clara, CA) in a stepwise gradient of ethyl acetate in hexanes (0–17 min, 0.6%; 17.01–42 minutes, 10%) at a flow rate of 1.4 mL·min$^{-1}$. Retinoids were detected by monitoring their absorbance at 325 nm and quantified based on a standard curve representing the relationship between the amount of synthetic retinoid standard and the area under the corresponding chromatographic peak. All procedures were done under dim red light.

All electrophysiology data is presented as mean ± SEM and all biochemical data is presented as mean ± SD. In all cases, the statistical significance was tested using two-tailed student's t-test. We used 5 *Gnat1*$^{-/-}$ and 5 WT mice as well as 1 cynomolgus monkey (two parafovea samples).

# RESULTS

## Physiological sensitivity of mammalian cones to far-red and near infrared light

We previously demonstrated that mouse rods in isolated retinas can respond robustly to 1000 nm stimulation via two-photon (2P) excitation of rhodopsin (Palczewska et al., 2014b). In the same study, we also recorded small responses from cones of *Gnat1*$^{-/-}$ mice. However, the lower efficiency of the previous experimental setup and significantly smaller responses of mammalian cones as compared to rods prevented a more precise quantitative determination of cone sensitivity to IR illumination. Here, we modified our device and experimental protocol to allow robust measurements of the sensitivity of mammalian cones at wavelengths longer than 730 nm, where the sensitivity of mouse M cones is ~5 log-units lower compared to their maximum sensitivity at 508 nm light (Nikonov et al., 2006). We used the specimen holder shown in Fig. 1A to image the flat-mounted retina. We recorded the cone component of the *ex vivo* transretinal electroretinogram (ERG) signal from *Gnat1*$^{-/-}$ mouse retina to stimuli ranging from visible light at 561 nm to near IR light at 1000 nm. At each of the wavelengths between 730 nm and 1000 nm the same tunable mode locked (pulsed) laser was used to stimulate photoreceptors with a short 10 ms scan over a 0.5 mm diameter circular area on the retina. Identical scanning parameters were also used to record responses to a 561 nm stimulus from a separate Diode Pumped Solid State (DPSS) laser. Fig. 1B shows an image of the stimulus area and highlights the circular area of the retina that contributed to the recorded electrical responses. The auto-fluorescence of fluorophores present in photoreceptor inner and outer segments allowed us to construct a 3D image of the stimulated retinal volume (Fig. 1C). A portion of the stimulus area of the retinas was imaged with 730 nm excitation light after each electrophysiological recording which allowed us to determine how well the z focus was aligned with the photoreceptor outer segments. This alignment is essential for optimizing the probability of 2P activation of the visual pigments as discussed below.

We determined the sensitivity (as described in Methods) of *Gnat1*$^{-/-}$ mouse cones at different wavelengths to a stimulus producing <30% of the maximal response at 561 nm (see Methods, Eq. 1). $R_{max}$ was set to that determined at 561 nm because it was not possible to saturate the cone photoresponse at all wavelengths. This analysis may have underestimated the sensitivity of cones to longer wavelengths where the maximal saturated response amplitude is probably smaller than measured when stimulating with traditional non-pulsing visible light ((Palczewska et al., 2014b) and below). The sensitivity at 561 nm was 0.006 ± 0.001% per photon $\mu m^{-2}$. Normalizing this by the cone collecting area of 0.078 $\mu m^2$ at 508 nm, as determined by Heikkinen et al. (Heikkinen et al., 2008), and multiplying it by 2.4 (1/0.42) to adjust for the decreased photoisomerization probability at 561 nm as compared to that at 508 nm, from the standard pigment template (Govardovskii et al., 2000), this corresponds to an estimated 0.2% of the maximal response produced by a single photoisomerization of the mouse cone M pigment. This value is consistent to that reported previously for homogenous flashes of non-pulsing light (Nikonov et al., 2006) and validates our assumption that photons delivered by the short 2D scan can simply be integrated as described in Methods (Eq. 2). Mouse cone responses to various stimulus intensities at different wavelengths are shown in Figs. 2A–D. Plotting the sensitivity S (Eq. 2 in Methods)

normalized to the sensitivity at 561 nm in a logarithmic scale as a function of wavelength, demonstrates that the sensitivity decreases only up to 800 nm and then slightly increases at 900 and 1000 nm (Fig. 3A). This is similar to what we found previously for rods (Palczewska et al., 2014b).

To allow more direct comparison of rod and cone data, we performed rod recordings from WT mice using the updated experimental setup. We found that in the updated setup under Ames' medium perfusion the half-maximal rod response required 16 photo-isomerizations (16 ± 3, n = 5), reflecting about 2-fold higher sensitivity as compared to our previous rod experiments conducted in HEPES-buffered Ringer's solution (Palczewska et al., 2014b) but consistent with other studies using Ames' medium (Azevedo and Rieke, 2011; Vinberg et al., 2014). Comparison to a 1-photon (1P) excitation pigment template revealed an important difference between rod and cone data. Whereas rod data (Fig. 3A, open triangles) accurately followed the template for 501 nm $\lambda_{max}$ pigment up to 800 nm (Govardovskii et al., 2000), the cone data diverged after 730 nm, suggesting again that nonlinear processes contributed to cone photoreceptor activation at wavelengths as low as 730 nm.

Two-photon absorption is inversely proportional to the laser pulse duration whereas 1P excitation should be independent of the pulse duration. Dispersion introduced by the components in the laser-light path results in elongation of the laser pulses. We previously estimated that in our two-photon electrophysiology system we can achieve approximately fourfold reduction in pulse duration by introducing dispersion compensation (Palczewska et al., 2014b). Thus, for the same stimuli power and pre-compensated pulses, we expected increase in electrophysiological responses for two-photon mediated process and no change in responses for one-photon process. We tested the effect of dispersion of the ultrashort laser pulses (in time domain) on cone activation efficiency at 800 and 1000 nm and found that dispersion of the laser pulses clearly reduced the efficiency of cone activation at these wavelengths (Fig. 3B). In contrast, turning the dispersion compensation OFF (i.e. introducing dispersion) at 730 nm, did not impact the response amplitudes of rod photoreceptors (Palczewska et al., 2014b). Together, these and previously published results indicate that nonlinear processes, namely 2P activation of cone visual pigments, contribute to cone activity at wavelengths as low as 730 nm in isolated mouse retinas. The most probable explanation is that, depending on the stimulus wavelength, the 2P activation of cone UV- and M-pigments contributes to or dominates the responses instead of traditional 1P excitation of the visual pigments above 730 nm and at least up to 1000 nm.

Next, we studied the sensitivity of primate photoreceptors to near IR stimulation in the parafovea of *ex vivo* retina samples as described in Methods. We obtained robust responses of macular cones to 561 nm (Fig. 4A) and 1000 nm (Fig. 4B) stimulation. The sensitivity (S) of macular cones to dim flashes at 561 nm in these experiments was about 1 log-unit lower as compared to *Gnat1*$^{-/-}$ cones. This may reflect the fact that the cones were not fully dark adapted after the bright light exposure during eye enucleation. It is also possible that the drugs used for euthanasia and the time between enucleation and experiments (> 2 h) were the cause of the lowered sensitivity observed in the macaque cones as compared to *Gnat1*$^{-/-}$ mouse cones. On the other hand, the maximal saturated *ex vivo* ERG responses from the parafoveal samples were about two times larger than the maximal responses recorded from

*Gnat1*$^{-/-}$ retina samples. This result is consistent with the higher density of cones, up to 35,000 cones per mm$^2$ in the recording area located within 0.5 mm from the fovea (Wikler et al., 1990; Pennesi et al., 2014), as compared to 12,200 cones per mm$^2$ across the whole mouse retina (Ortin-Martinez et al., 2014). The responses from parafoveal samples also provided evidence of a slower component, likely originating from rods. However, the contribution of the slow rod-driven response to the amplitudes of the *ex vivo* ERG responses in the macular samples appeared to be very small. Fig. 4C plots normalized responses to 10 ms dim light flashes at 561 nm from wild type (WT) mouse rods (black), parafoveal macaque cones (red) and *Gnat1*$^{-/-}$ mouse cones (green). The mouse rod responses were clearly slower than those recorded from *Gnat1*$^{-/-}$ mouse and macaque macula retina samples. This suggests that the responses in our macaque recordings were dominated by cone photoreceptors. Furthermore, the responses to test flashes in the green section of the visible spectrum as well as those of near IR light would be expected to be driven almost exclusively by M/L cones due to the lower density and spectral sensitivity of S cones at these wavelengths. To compare the spectral sensitivity of photoreceptors at far red and near infrared in WT and *Gnat1*$^{-/-}$ mouse retinas as well as in macaque macula samples, we examined their sensitivity normalized to the sensitivity at 561 nm ($S_\lambda$/S561nm) as a function of wavelength (Fig. 5A). The recorded data were compared to the predicted 1P spectral sensitivity functions (Govardovskii et al., 2000) for mouse rod ($\lambda_{max}$ = 501 nm, dashed black line), mouse M cone ($\lambda_{max}$ = 508 nm, dashed green line) as well as a 85%/15% mixture of M cone ($\lambda_{max}$ = 530 nm) and L cone ($\lambda_{max}$ = 560 nm) pigments (dashed red line). As discussed above, the rod data followed the predicted 1P spectral sensitivity template accurately up to 800 nm whereas the *Gnat1*$^{-/-}$ mouse cone data demonstrated higher than expected sensitivities above 730 nm. The relative predicted 1P sensitivity at longer wavelengths compared to that measured at 561 nm was significantly lower than the actual measurement for all wavelengths larger than 730 nm ($p<0.03$; 2-tailed paired t-test, n = 5). The macaque cone data also diverged from the 1P pigment template for stimuli above 800 nm. By performing 2P imaging, we confirmed that the analyzed retinal samples were from the parafovea. Fig. 5B shows a 3D reconstruction of the parafoveal region of the right eye. The strong auto-fluorescence, probably from 2P excitation of NADPH and all-*trans*-retinol (Sharma et al., 2016) revealed inner segments of cone photoreceptors. The fluorescence of 11-*cis*-retinal is negligible because its quantum yield is less than $5{\cdot}10^{-4}$ (Becker et al., 1971; Becker et al., 1976) as compared to the fluorescence of retinol whose quantum yield is higher than 0.01 (Palczewska et al., 2014a). Fig. 5C shows a 2D image of the rod and cone outer segments from a peripheral region of the same retina, revealing a much larger spacing between the cones (average 16.2 μm, with S.D. of 2.8 μm) as compared to the parafoveal (cone spacing on average 9.0 μm and S.D. 1.4 μm).

## Retinoid analyses in cynomolgus macaque retinal tissue

To verify that our macaque retinal samples were not bleached and to characterize their retinoid content, we measured the amount of *cis* and *trans* isomers of retinal, retinyl esters and retinols in the retina and RPE by HPLC (Fig. 6). We used portions of the macaque retina that were not used for ERG measurements. We found substantial quantities of 11-*cis*-retinal in the retina and 9-fold lower levels in the RPE. We found both *trans* and *cis* isomers of retinyl esters in the samples containing RPE but not in the retina. As expected for primate

eye, both isomers of retinol were present in the retina and to a lesser degree, ~5 times less, in the RPE. These results confirmed the viability of retinal tissue samples for ERG measurements.

## DISCUSSION

It has been appreciated for decades that humans can perceive light of wavelengths outside the canonical “visible range” of 400 to 700 nm, particularly in the far-red and near IR part of the spectrum (Griffin et al., 1947; Walraven and Leebeek, 1963; Sliney et al., 1976; Dmitriev et al., 1979). We recently demonstrated that in mammalian rods, the detection and perception of near IR light occurs via a 2-photon excitation. In this scenario, two photons of near IR light are absorbed simultaneously by a single visual pigment molecule and their combined energy results in its activation and visual perception identical to the perception of a single photon with equivalent energy (Palczewska et al., 2014b). Rods dominate visual perception in dim light condition but are largely saturated during the day, making it unlikely that their activation by near IR light from a bright enough source will have functional consequences. In contrast, cones mediate daytime perception and are able to function in much brighter conditions, possibly including substantial near IR stimulation. Thus, here, we sought to determine whether mammalian cone photoreceptors can also be activated by near IR light and if so, whether this occurs by a 2P excitation mechanism similar to that described previously in mammalian rods.

Using mice with disabled rod signal transduction, and the parafoveal region of cynomologus, we demonstrated that cone photoreceptors like rods are also responsive to 2P excitation/isomerization. Several observations indicate that these cone responses arise from 2P excitation of cone visual pigments. First, the sensitivity of mouse and primate cones diverged from the predicted 1P activation template for wavelengths above 768 nm and 800 nm, respectively (Figs. 3A and 5A), indicating a shift in the activation mechanism from 1P in visible light to 2P in near IR light. Second, the pulse duration of laser illumination had a strong effect on cone sensitivity at 800 (Fig. 3B, top) and 1000 nm (Fig. 3B, bottom) in Gnat1−/− mouse retinas, and at 1000 nm in primate cones (inset of Fig. 4B). Decreasing pulse duration increased response amplitudes substantially, indicating the involvement of a non-linear 2P process in the activation of their visual pigment. Although nonlinearity could also arise from second harmonic generation and/or fluorescence light from 2P excitation of molecules in the retina, these are not probable explanations for the ERG IR sensitivity of cones at 1000 nm. The fluorescence signal that we detected from the retinas when imaged at 730 nm was very weak at 1000 nm, and probably originated from NADH and/or retinoids. Further, we did not detect any second harmonic generation in the retina (Palczewska et al., 2014b). Interestingly, when compared to visible light, mouse cone sensitivity to IR was higher than that of rods (Fig. 3A). Similarly, primate cones appeared to be more sensitive to IR relative to the VIS stimulus when compared to mouse rods (Fig. 5A). It is possible that the 2P action spectra of the cone pigments (which are not known) are different from that of rhodopsin, giving rise to the higher IR sensitivity of cones compared to rods. Alternatively, their shorter outer segments could make it more likely to achieve efficient focus and uniform 2P stimulation in cones than in rods.

According to Wald and colleagues, the peripheral retina is about 13 log units more sensitive to 500 nm light as compared to that at 1050 nm (Griffin et al., 1947). Recent work, however, has shown that 'turning-on' 2P vision increases IR sensitivity by several log units above the level expected from one-photon excitation (Palczewska et al., 2014b). This creates the possibility of using pulsed near IR stimulation to study visual perception and the function of the retina in humans. Although 1P and 2P vision can result in almost identical vision sensations, *i.e.* green light perception during stimulation with either short pulses of IR at 1045 nm or 523 nm light (Palczewska et al., 2014b), there are advantages for choosing an IR stimulus. Infrared light is absorbed and scattered less in the eye in comparison to visible light, allowing longer wavelengths of light to penetrate deeper into biological tissues. This would enable accurate measurements of visual sensitivity within a well-defined region of the eye. In addition, the narrow activation zone of 2P excitation combined with the use of infrared light would allow local measurements of photoreceptor sensitivity without inducing a substantial bleach of the visual pigment. Such a scenario should allow simultaneous measurements of photoreceptor sensitivity and retinoid content in the intact human retina during dark adaptation. As this process is compromised or delayed in a wide range of visual disorders from Oguchi and Stargardt's diseases (Lamb and Pugh, 2004), retinitis pigmentosa (Omar and Herse, 2004), AMD (Owsley et al., 2016), and even normal aging (Coile and Baker, 1992; Gaffney et al., 2012), our findings could lead to the development of experimental and diagnostic tools to better understand the link between dark adaptation and blinding disorders in general.

## ACKNOWLEDGMENTS

We thank members of the Palczewski laboratory for valuable comments regarding this manuscript. This research was supported in part by grants from the National Institutes of Health (NIH) EY027283 (K.P. and V.J.K), EY025451 (K.P. and V.J.K.), EY019312 (V.J.K), EY026651 (F.V.), and EY02687 to the Department of Ophthalmology and Visual Sciences at Washington University, and by Research to Prevent Blindness. M.W. would like to acknowledge the European Union's Horizon 2020 research and innovation programme grant No. 666295 and the TEAM TECH/2016–3/20 programme of the Foundation for Polish Science co-financed by the European Union under the European Regional Development Fund.

## ABBREVIATIONS

| | |
|---|---|
| **1P** | one-photon |
| **2P** | two-photon |
| **AMD** | age-related macular degeneration |
| **DPSS** | diode pumped solid state |
| **ERG** | electroretinogram |
| **IR** | infrared |
| **RP** | retinitis pigmentosa |
| **RPE** | retinal pigment epithelium |
| **VIS** | visible |

**WT** wild type

## REFERENCES


Ambati J, Fowler BJ (2012) Mechanisms of age-related macular degeneration. Neuron 75:26–39. [PubMed: 22794258]

Azevedo AW, Rieke F (2011) Experimental protocols alter phototransduction: the implications for retinal processing at visual threshold. J Neurosci 31:3670–3682. [PubMed: 21389222]

Becker RS, Inuzuka K, King J, Balke DE (1971) Comprehensive investigation of the spectroscopy and photochemistry of retinals. II. Theoretical and experimental consideration of emission and photochemistry. J Am Chem Soc 93:43–50. [PubMed: 5538868]

Becker RS, Hug G, Das PK, Schaffer AM, Takemura T, Yamamoto N, Waddell W (1976) Visual Pigments .4. Comprehensive consideration of spectroscopy and photochemistry of model visual pigments. J Phys Chem-Us 80:2265–2273.

Coile DC, Baker HD (1992) Foveal dark adaptation, photopigment regeneration, and aging. Vis Neurosci 8:27–39. [PubMed: 1739675]

Crawford BH (1949) The scotopic visibility function. Proceedings of the Physical Society B 62:321–334.

Curcio CA, Sloan KR, Kalina RE, Hendrickson AE (1990) Human photoreceptor topography. J Comp Neurol 292:497–523. [PubMed: 2324310]

Curcio CA, Sloan KR Jr., Packer O, Hendrickson AE, Kalina RE(1987) Distribution of cones in human and monkey retina: individual variability and radial asymmetry. Science 236:579–582. [PubMed: 3576186]

Dmitriev VG, Emelyanov VN, Kashintser MA, Kulikov V, Solver AAVV, Stelmakh MF, Cheredrichenko OB (1979) Nonlinear perception of infra-red radiation in the 800–1355 nm range with human eye. Sov J Quantum Electron 9:475–479.

Gaffney AJ, Binns AM, Margrain TH (2012) Aging and cone dark adaptation. Optom Vis Sci 89:1219–1224. [PubMed: 22773176]

Govardovskii VI, Fyhrquist N, Reuter T, Kuzmin DG, Donner K (2000) In search of the visual pigment template. Vis Neurosci 17:509–528. [PubMed: 11016572]

Griffin DR, Hubbard R, Wald G (1947) The sensitivity of the human eye to infra-red radiation. J Opt Soc Am 37:546–554. [PubMed: 20256359]

Heikkinen H, Nymark S, Koskelainen A (2008) Mouse cone photoresponses obtained with electroretinogram from the isolated retina. Vision Res 48:264–272. [PubMed: 18166210]

Kraft TW, Schneeweis DM, Schnapf JL (1993) Visual transduction in human rod photoreceptors. J Physiol 464:747–765. [PubMed: 8229828]

Lamb TD, Pugh EN Jr. (2004) Dark adaptation and the retinoid cycle of vision. Prog Retin Eye Res 23:307–380. [PubMed: 15177205]

Masland RH (2012) The neuronal organization of the retina. Neuron 76:266–280. [PubMed: 23083731]

Mustafi D, Engel AH, Palczewski K (2009) Structure of cone photoreceptors. Prog Retin Eye Res 28:289–302. [PubMed: 19501669]

Nikonov SS, Kholodenko R, Lem J, Pugh EN Jr. (2006) Physiological features of the S- and M-cone photoreceptors of wild-type mice from single-cell recordings. J Gen Physiol 127:359–374. [PubMed: 16567464]

Omar R, Herse P (2004) Quantification of dark adaptation dynamics in retinitis pigmentosa using non-linear regression analysis. Clin Exp Optom 87:386–389. [PubMed: 15575812]

Ortin-Martinez A, Nadal-Nicolas FM, Jimenez-Lopez M, Alburquerque-Bejar JJ, Nieto-Lopez L, Garcia-Ayuso D, Villegas-Perez MP, Vidal-Sanz M, Agudo-Barriuso M (2014) Number and distribution of mouse retinal cone photoreceptors: differences between an albino (Swiss) and a pigmented (C57/BL6) strain. PloS one 9:e102392. [PubMed: 25029531]

Owsley C, McGwin G, Clark ME, Jackson GR, Callahan MA, Kline LB, Witherspoon CD, Curcio CA (2016) Delayed rod-mediated dark adaptation is a functional biomarker for incident early age-related macular degeneration. Ophthalmology 123:344–351. [PubMed: 26522707]

Palczewska G, Kern TS, Palczewski K (2019) Noninvasive two-photon microscopy imaging of mouse retina and retinal pigment epithelium. Methods Mol Biol 1834:333–343. [PubMed: 30324453]

Palczewska G, Golczak M, Williams DR, Hunter JJ, Palczewski K (2014a) Endogenous fluorophores enable two-photon imaging of the primate eye. Invest Ophthalmol Vis Sci 55:4438–4447. [PubMed: 24970255]

Palczewska G, Vinberg F, Stremplewski P, Bircher MP, Salom D, Komar K, Zhang J, Cascella M, Wojtkowski M, Kefalov VJ, Palczewski K (2014b) Human infrared vision is triggered by two-photon chromophore isomerization. Proc Natl Acad Sci USA 111:E5445–5454. [PubMed: 25453064]

Pennesi ME, Garg AK, Feng S, Michaels KV, Smith TB, Fay JD, Weiss AR, Renner LM, Hurst S, McGill TJ, Cornea A, Rittenhouse KD, Sperling M, Fruebis J, Neuringer M (2014) Measuring cone density in a Japanese macaque (Macaca fuscata) model of age-related macular degeneration with commercially available adaptive optics. Adv Exp Med Biol 801:309–316. [PubMed: 24664712]

Rivolta C, Sharon D, DeAngelis MM, Dryja TP (2002) Retinitis pigmentosa and allied diseases: numerous diseases, genes, and inheritance patterns. Hum Mol Genet 11:1219–1227. [PubMed: 12015282]

Sharma R, Williams DR, Palczewska G, Palczewski K, Hunter JJ (2016) Two-photon autofluorescence imaging reveals cellular structures throughout the retina of the living primate eye. Invest Ophthalmol Vis Sci 57:632–646. [PubMed: 26903224]

Sliney DH, Wangemann RT, Franks JK, Wolbarsht ML (1976) Visual sensitivity of the eye to infrared laser radiation. J Opt Soc Am 66:339–341. [PubMed: 1262982]

Vinberg F, Kefalov V (2015) Simultaneous ex vivo functional testing of two retinas by in vivo electroretinogram system. J Vis Exp:e52855. [PubMed: 25992809]

Vinberg F, Kolesnikov AV, Kefalov VJ (2014) Ex vivo ERG analysis of photoreceptors using an in vivo ERG system. Vision Res 101:108–117. [PubMed: 24959652]

Walraven PL, Leebeek HJ (1963) Foveal sensitivity of the human eye in the near infrared. J Opt Soc Am 53:765–766. [PubMed: 13998626]

Wikler KC, Williams RW, Rakic P (1990) Photoreceptor mosaic: number and distribution of rods and cones in the rhesus monkey retina. J Comp Neurol 297:499–508. [PubMed: 2384610]

Zipfel WR, Williams RM, Webb WW (2003) Nonlinear magic: multiphoton microscopy in the biosciences. Nat Biotechnol 21:1369–1377. [PubMed: 14595365]

## Highlights

- Mouse and primate cone photoreceptors can respond to infrared light stimulation
- Cone sensitivity to near IR light exceeds the predicted 1-photon sensitivity
- Detection of IR light is dependent on minimizing light pulse duration
- Mammalian cones are activated by near IR light by nonlinear 2-photon excitation

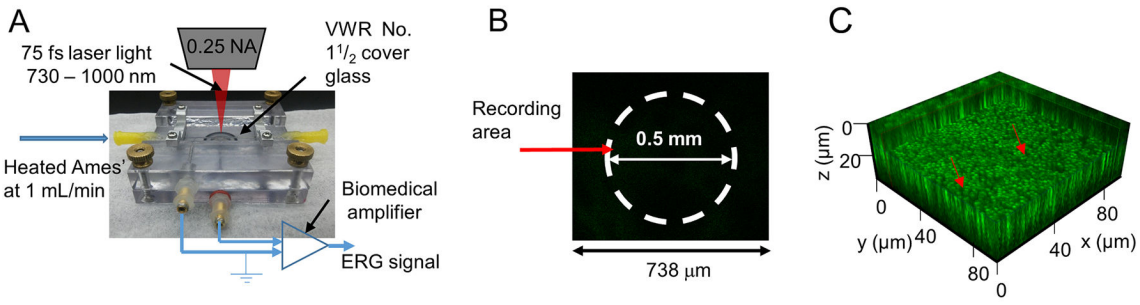


**Figure 1. Improved device and experimental protocol for IR stimulation of mammalian cones.**

(A) Custom-built specimen holder allowing simultaneous two-photon (2P) imaging and *ex vivo* ERG recording. Stimuli were provided by a tunable mode-locked Ti:Sapphire and 561 nm laser beams for a 10 ms scanning time. (B) A laser beam scanned a 738 × 738 μm area of the retina, and ERG responses were collected from a 0.5 mm diameter circle within the scanning area. (C) 3D volume reconstruction of the Z-stack of 2P excited fluorescence images from the ERG recording volume. Z=0 μm is just above the tips of photoreceptor outer segments. Red arrows point to column-like outer segments.

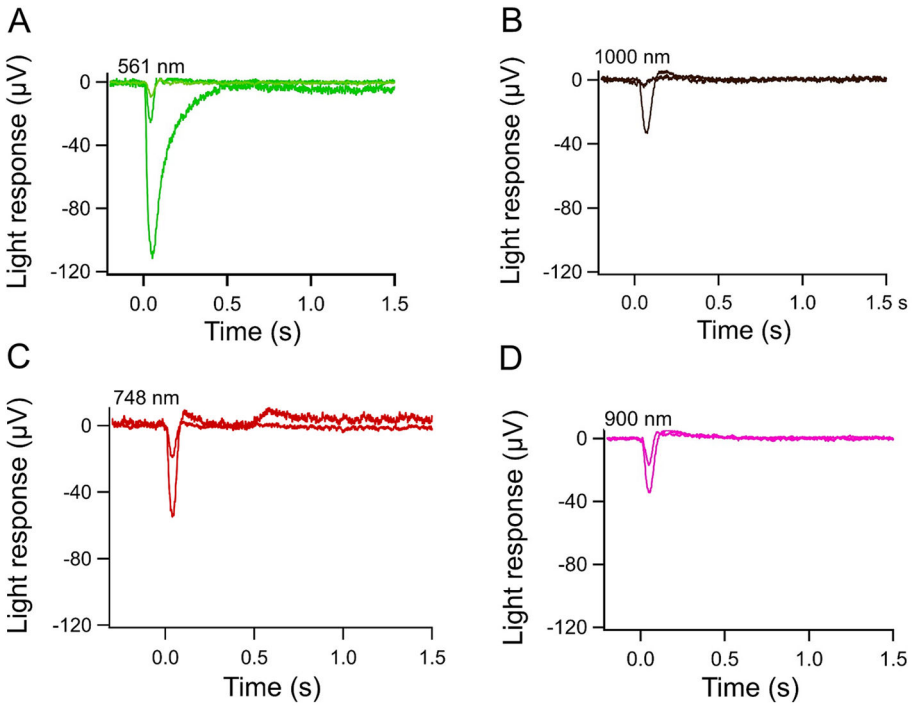


**Figure 2. Cones in isolated mouse retina can respond robustly to 730 – 1000 nm light stimulation.**
Representative *ex vivo* ERG cone responses to 561 nm (A), 1000 nm (B), 748 nm (C), and 900 nm (D) stimulation from the same *Gnat1*$^{-/-}$ retina shown in Fig. 1.

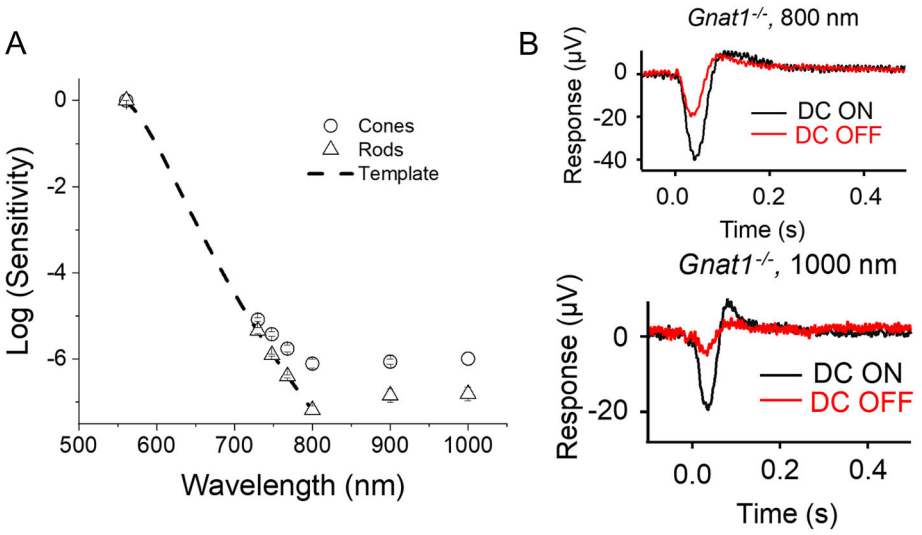


**Figure 3. Spectral sensitivity of mouse cones above 730 nm is higher than predicted by the 1-photon spectral template.**

(A) Sensitivity ($S_\lambda$) determined as described in Methods plotted as a function of stimulus wavelength (open circles, *Gnat1*$^{-/-}$ mice, n = 5; open triangles, WT mice, n = 5). The absolute sensitivity of rods was about two log-units lower than cones. Data were normalized to their sensitivity at 561 nm to facilitate a comparison between rods and cones. The dashed line plots the expected sensitivity at each wavelength, based on the 1P excitation template for rhodopsin (Govardovskii et al., 2000). (B) Impact of turning off the dispersion compensation (DC) at 800 and 1000 nm.

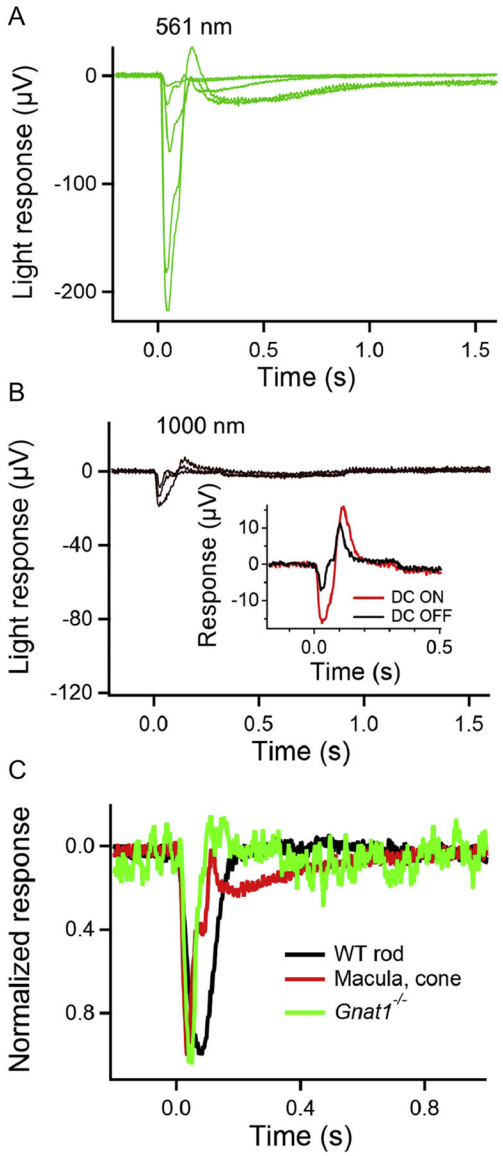


**Figure 4. Cones in isolated primate retina can respond robustly to 1000 nm light stimulation.**

Light responses recorded from a parafoveal sample of the right eye (dark-adapted eye cup, no 11-*cis*-retinal incubation) from a cynomologus monkey at 561 nm (A) and 1000 nm (B). The calculated light intensities were $3.9\times10^3$, $9.7\times10^3$, $5.8\times10^4$, $5.35\times10^5$, $2.57\times10^6$ photons $\mu m^{-2}$ at 561 nm and $1.4\times10^9$, $2.3\times10^9$, and $3.8\times10^9$ photons $\mu m^{-2}$ at 1000 nm. The inset in (B) plots responses to a stimulus identical in average power, with dispersion compensation either turned ON (red) or OFF (black) at 1000 nm. (C) Normalized responses to a 561 nm stimulus producing <20% of the maximal saturated photoresponse from mouse rods (black), mouse cones (*Gnat1*$^{-/-}$; green) and from the parafovea of a cynomolgus monkey retina (red).

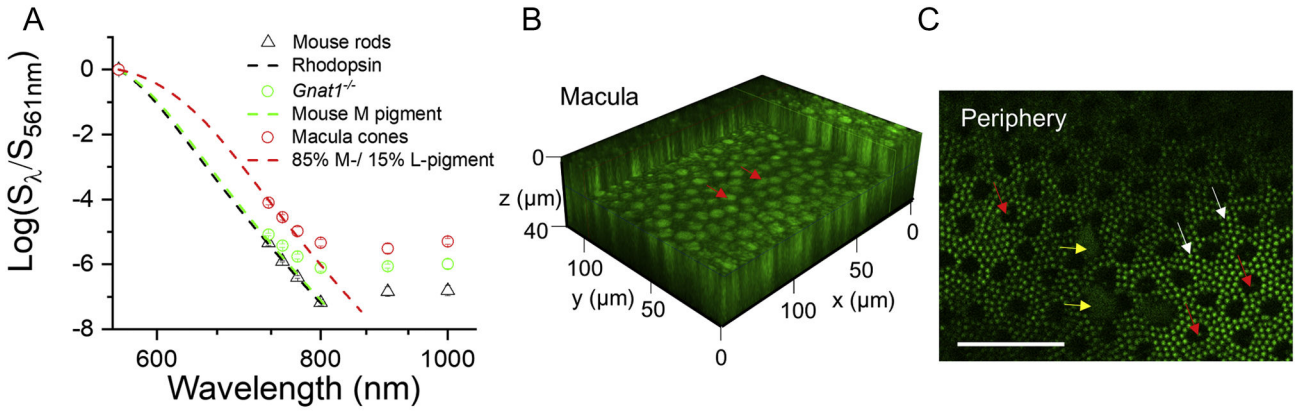


**Figure 5. Imaging of photoreceptors from primate retina during IR recordings.**

(A) Sensitivity of primate parafoveal photoreceptors normalized to the sensitivity at 561 nm (open red circles, n = 2 retina samples, 1 macaque) is compared to that recorded from mouse rods (open black triangles, n = 5) and mouse cones (*Gnat1*$^{-/-}$; open green circles, n = 5). The dashed lines show the expected sensitivity based on rhodopsin (501 nm, black), mouse cone M pigment (508 nm, green), and a mix of 85% macaque M- (530 nm) and 15% L-pigment (560 nm) 1P templates (Govardovskii et al., 2000) (red). (B) 3D reconstruction based on the 2P imaging data obtained with 730 nm excitation light from the parafovea of a cynomologus monkey retina that was subject to IR stimulation to produce the responses in Fig. 4. Red arrows indicate cone inner segments. (C) 2D image obtained with laser light focused on the outer segments and showing rod (white arrows) and faintly visible cone outer segments tips (red arrows) from a peripheral retina sample of the same right eye shown in A, B, and C. Yellow arrows indicate portions of RPE cells that adhered to the retina after retinal separation. Scale bar, 50 μm.

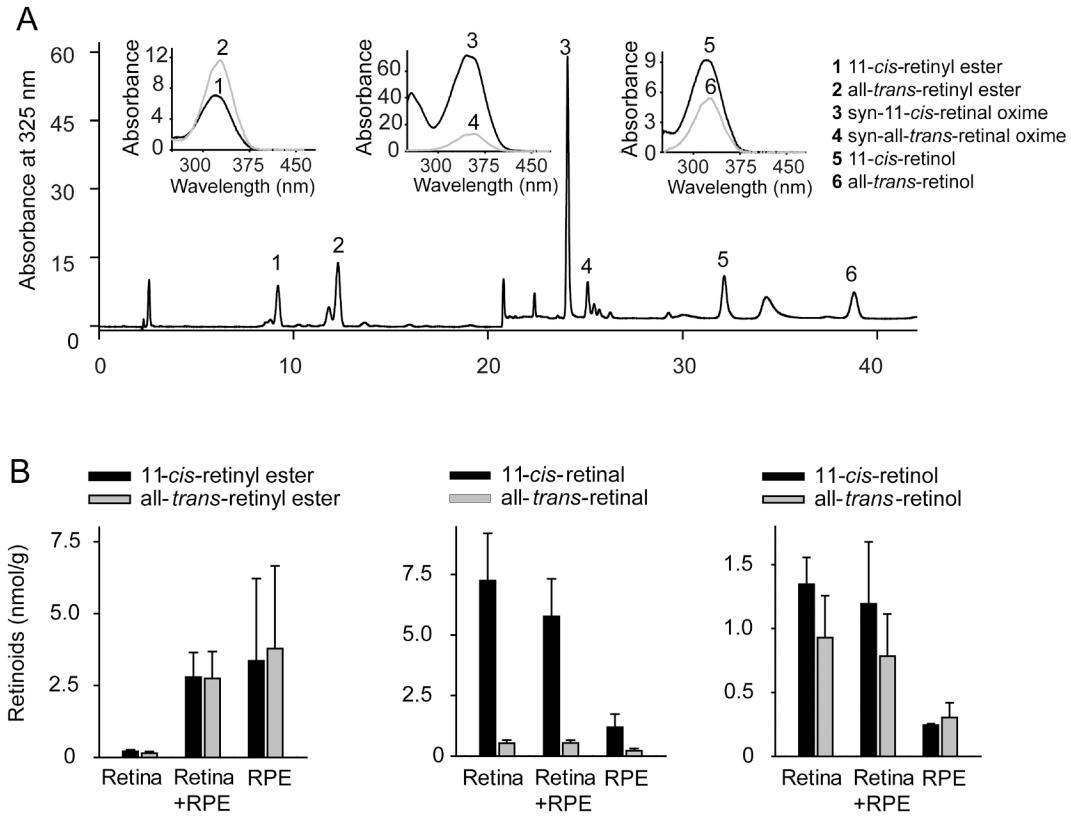


**Figure 6. Quantification of retinoid levels in cynomolgus macaque RPE and retina.**

(A) A representative HPLC chromatograph of retinoid extracts from a sample of retina and RPE is shown. Peaks **1–6** represent 11-*cis*-retinyl ester, all-*trans*-retinyl ester, *syn*-11-*cis*-retinal oxime, *syn*-all-*trans*-retinal oxime, 11-*cis*-retinol and all-*trans*-retinol respectively. The insets represent the corresponding UV spectra of these peaks. (B) Levels of retinyl esters (left), retinals (middle) and retinols (right) in retina, a mixture of retina and RPE, or RPE alone. All values were normalized to nmol per gram sample. Each group contains 2–3 samples from different left and right eyes. Error bars represent standard deviations.